THE INTERNATIONAL JOURNAL OF MEDICAL ROBOTICS AND COMPUTER ASSISTED SURGERY
Int J Med Robotics Comput Assist Surg 2011; **7**: 334–347.
Published online 5 July 2011 in Wiley Online Library (wileyonlinelibrary.com) **DOI:** 10.1002/rcs.403

ORIGINAL ARTICLE

Control design and implementation of a novel master–slave surgery robot system, MicroHand A

Hongqiang Sang
Shuxin Wang*
Jianmin Li
Chao He
Lin'an Zhang
Xiaofei Wang

School of Mechanical Engineering, Tianjin University, People's Republic of China

*Correspondence to: Shuxin Wang, School of Mechanical Engineering, Tianjin University, Tianjin 300072, People's Republic of China. E-mail: shuxinw@tju.edu.cn

Accepted: 18 April 2011

Abstract

Background Compared with conventional minimally invasive surgery and open surgery, robotic-assisted minimally invasive surgery can overcome or eliminate drawbacks caused by operator restrictions, motion limitation by the trocar and the image system, such as fatigue, trembling, low precision, constrained degree-of-freedom, poor hand–eye coordination and restricted surgical vision. In this paper, a novel partly tendon-driven master–slave robot system is proposed to assist minimally invasive surgery and a master–slave control architecture is developed for abdominal surgical operations.

Methods A novel master–slave surgery robot system named MicroHand A has been developed. A kinematic analysis of master and slave manipulators was conducted, based on screw theory and vector loop equation. The relationships of the tendon-driven multi-DOF surgical instrument among Cartesian space, actuator space and joint space were derived for control purposes. The control system architecture of the MicroHand A was designed with intuitive motion control and motion scaling control. Llewellyn's absolute stability criterion and the transparency of the one-DOF master–slave system are also analysed.

Results Intuitive motion control under dissimilar kinematics in master–slave manipulations and motion scaling control were accomplished to solve absonant hand–eye coordination, kinematic dissimilarity and workspace mismatch of master–slave manipulator problems. A series of tests and animal experiments were carried out to evaluate system performance. The experimental results demonstrate that the system could accomplish intuitive motion control and motion scaling control, and that the control system is stable and reliable.

Conclusions The experiments performed on the MicroHand A robotic system yielded expected control results. The system satisfies the requirements of minimally invasive surgery. Intuitive motion control and motion scaling control under different kinematics for the master and slave have been implemented. Copyright © 2011 John Wiley & Sons, Ltd.

Keywords minimally invasive surgery; tendon-driven; kinematic; master–slave control; intuitive motion control

Introduction

Unlike traditional surgery, minimally invasive surgery adopts special instruments and operational techniques to reduce patient trauma. It is usually performed by long and thin instruments and a camera, such as an endoscope,

both of which are inserted into the patient's body through small incisions. Compared with open surgery there are many advantages for patients, such as less pain, smaller scarring, less injury to tissue, less blood loss, and shorter rehabilitation and hospitalization times. However, there are also many disadvantages for surgeons, including a constrained degree of freedom, more restricted surgical vision, existing leverage effect, no force feedback, unavoidable manual tremor, easier tearing of skin or soft tissues, and a long learning curve (1).

Robot-assisted minimally invasive surgery technology has been introduced into the operating room in order to overcome or eliminate most of the drawbacks of traditional minimally invasive surgery. Robot-assisted minimally invasive surgery systems have been developed. There are two typical commercially available systems. The first is the da Vinci system, produced by Intuitive Surgical Inc., and it has been used worldwide for many surgical procedures, including urological surgery, general laparoscopic surgery, gynaecological laparoscopic surgery and cardiac surgery (2–6). It can provide three-dimensional (3D) images, interchangeable two-DOF wrist instruments with a diameter of 8 or 5 mm, and force feedback to surgeon by integrated sensors on the shafts of the surgical instruments, although not clinically applicable. The system allows surgeon hand–eye coordination, eliminates surgeon tremor and realizes motion scaling. The second is the Zeus system, produced by Computer Motion Inc. (7). It can execute voice command in addition to tremor elimination and motion scaling.

At research institutes, some minimally invasive robotic surgery systems have also been developed. UC Berkeley and UC San Francisco developed a complete prototype robotic system for telesurgery (8). The slave has six degrees of freedom (DOFs) for full manipulability and the master has the capability of four-DOF force feedback. Due to the lack of force feedback in certain DOFs from the slave manipulator, the end effector was damaged during *in vitro* experimental trials. The Korea Advanced Institute of Science and Technology developed a telepresence system (9). The master has six-DOF force/torque reflection. The slave is composed of a six-DOF industrial robot and a modified six-DOF Stewart platform applied for micromanipulation. However, the system can not be used in surgery because clinical situations are not considered in industrial robot design. An advanced robotics and telemanipulator system for minimally invasive surgery was developed by Karlsruhe Research Centre, Germany (10,11). The end effector can bend $>180^\circ$ and accurately position the tip. The master control involves weight and friction compensations, motion scaling and force feedback features. Programs in the system provide surgeons with the ability to monitor and control the robot. Boundaries can prevent surgeons from engaging sensitive areas via software settings. A 3D simulator offers additional information to surgeons. The results of experiments on animals show that the system has a bright future. The Hyper Finger robotic system was developed by Nagoya University (12). The system is small and light enough to be mounted on a camera tripod stand. The slave has nine DOFs to help the surgeon control the gripper's movement smoothly. The master is kinematically similar to the slave. After *in vivo* experiments on a pig, the system was found to be easy to control. Another robotic system from Nagoya University can perform surgery in deep and narrow spaces (13). The slave can reach deep and narrow spaces by means of a 3 mm diameter end effector and its flexible body trunk. The master offers good operability and controllability for the slave. Suturing on chicken livers has been successfully performed. The RobIn heart (14) slave manipulator has seven DOFs for motion control and one DOF for grapping. One redundant DOF near the wrist increases manoeuvrability and avoids conflicts with obstacles. The system can prevent breakdown if one or more tendons break. Different masters, such as a modified computer joystick, a keyboard and a haptic laparoscopic master robot being capable of providing one DOF force feedback, are used to control the slave. The robotic systems mentioned above are far from being completed.

Since most hospitals in China can not afford the high cost of the da Vinci system, the MicroHand A system was developed especially for the Chinese market. It was not a simple copy but a challenge to develop an improved version of the above-mentioned robots, at least in one aspect.

In this paper, the Materials and methods section introduces the design requirements and an overview of the MicroHand A system. The kinematics analyses performed include master forward kinematics, slave forward and inverse kinematics after removing tendons, and multi-DOF tendon-driven instrument kinematics. The intuitive control algorithm, the open-and-close algorithm and control system design are also described in this section. The stability conditions that meet Llewellyn's absolute stability criterion and transparency of one-DOF master–slave system are also analysed. Experimental results are presented in Experiments and Results to demonstrate the validity of the proposed control system, which accomplishes intuitive motion control and motion scaling control under kinematically dissimilar master–slave manipulations. Finally, our conclusions and proposals for future work are given in the Discussion.

Materials and Methods

Design requirements

In laparoscopic surgery, the abdominal wall is expanded by inflating with carbon inside to expose and access the operating field. Three small incisions are made to allow instruments and an endoscope to enter into the body, as shown in Figure 1. By constraints of the incision point, the instrument shaft is limited to having only four DOFs.

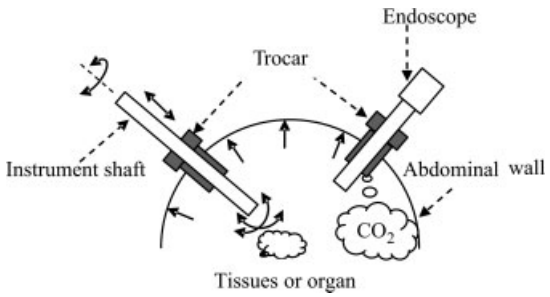

Figure 1. The incision point constraints

Thus, mechanical design issues according to minimally invasive surgery requirements are considered as follows:

(a) *The remote centre of motion*. Due to the incision constraints and the requirement to minimize injury at the incision point, it is required that the axis of a distal instrument of the manipulator must always pass through the incision point. That is to say, the robotic manipulator has an effective rotation centre at the incision point.
(b) *Multi-DOF instruments with a compact wrist mechanism*. Three additional DOFs are added to the distal instruments by a tendon-driven system. The additional DOFs give enough dexterity for the robotic system to perform complex surgical procedures, such as suturing and knot-tying, in a minimally invasive surgery environment, and the instruments are able to exert forces large enough to grip needles and manipulate tissues. Of course, the surgical instruments can also be sterilized.
(c) *Rapid instrument changing*. Surgical operations usually require many different surgical instruments. Fast instrument changing can shorten surgical operation time.
(d) *Backdrivability*. Backdrivability permits surgeons to move the manipulator directly under manual control, which is critical for removing the robot from the patient in a case of operation failure.

Current prototype

A novel robot-assisted minimally invasive surgery system, MicroHand A, has been set up by Tianjin University according to the requirements and the necessary conditions of minimally invasive surgery. Figure 2 shows the structure of the MicroHand A system, including two master manipulators, two slave instrument manipulators and one slave endoscope manipulator.

The master manipulator with seven DOFs is a serial robot, as shown in Figure 3. Joints 1, 2 and 3 are used as positional degrees of freedom. The axes of wrist joints intersect at a common point, greatly simplifying the kinematic analysis and effectively decoupling the position and orientation. The master manipulator can perceive the surgeon's hand motions, put these motions into position signals and provide force and tactile feedback.

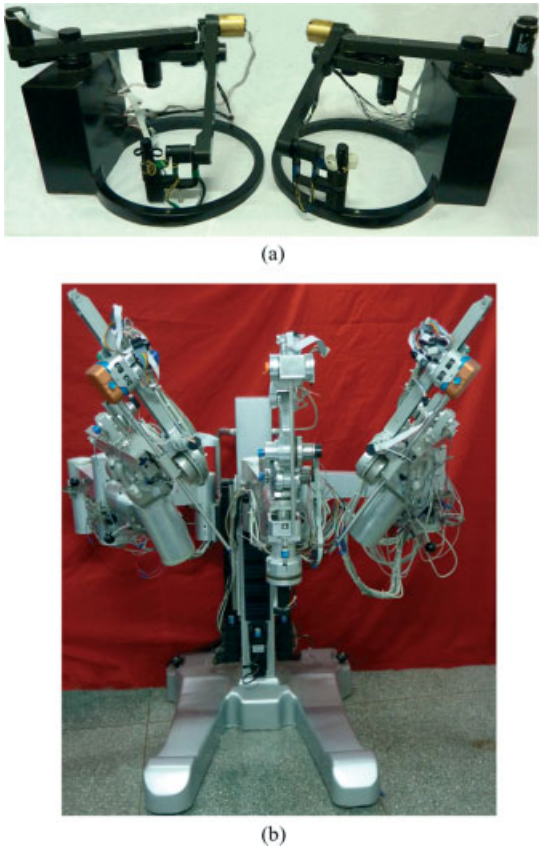

Figure 2. MicroHand A surgical robotic system: (a) master manipulators; (b) slave manipulators

This means that the master manipulator can provide three-DOF position information in the Cartesian space, three-DOF rotation information, three-DOF force output and one-DOF open-and-close control for grapping. Force output function has been applied in surgery simulation. Currently, the three-DOF force output function is reserved due to the absence of force information in the slave manipulators in this study.

Each slave instrument manipulator is composed of two parts. One is a six-DOF passive part for rapid adjustment before surgery. It is installed on the base of the slave manipulator. The other is an active part, including a novel remote centre of motion mechanism that can provide three DOFs for positioning multi-DOF instruments. The multi-DOF instruments can provide enough dexterity to perform complex surgical operations, such as suturing and knot-tying tasks.

The prototype of the passive arm is shown in Figure 4. It is composed of one active joint, one translation joint, T, and five passive revolution joints, R_1 to R_5.

The remote centre of motion can be implemented with several mechanical designs, such as spherical joints, spherical link mechanisms and double-parallelogram mechanisms (15–17). The prototype of the remote centre of motion mechanism is shown in Figure 5. It is composed of three active joints, one revolution joint, R, and two translation joints, T_1 and T_2. The revolution joint R_p and the translation joint T_p are passive joints to provide

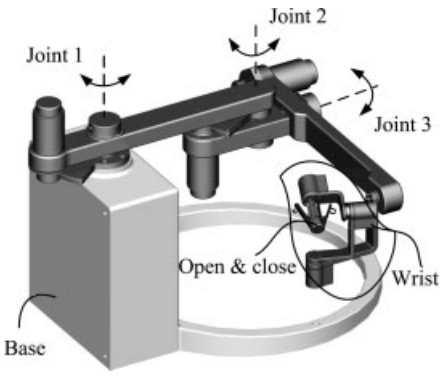

Figure 3. The master manipulator with seven DOFs

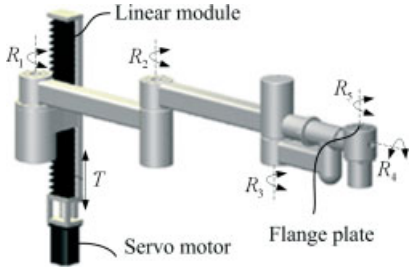

Figure 4. Passive arm

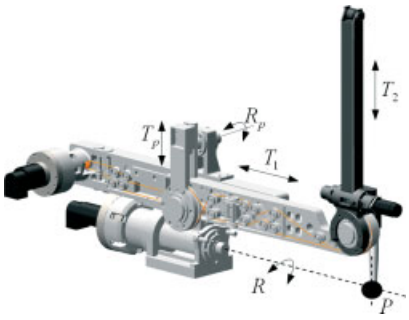

Figure 5. The remote centre of motion mechanism

constraints. The mechanism is installed on the flange plate of the passive arm. The design principle and model derivation of the novel remote centre of motion mechanism can be found in (18).

Multi-DOF instruments with a compact wrist mechanism are shown in Figure 6. It is small and can provide a wide range of motion and a relatively large force to implement complex operations. A grasping force of >12 N can be provided for clamping needles. The amplitude factor of grasping force is set by the controller according to different task requirements. These DOFs of the instrument are actuated by a tendon–pulley system and DC servo-motors located at the remote centre of motion mechanism. The range of the roll motion is from −170° to 170°; the pitch motion and the yaw motion are from −90° to 90°. The open-and-close angle is in the range 0–80°.

The endoscope manipulator is also composed of two parts. One is a holding endoscope part and the other is a six-DOF passive part for rapid adjustment before surgery. The passive part is the same as that of the

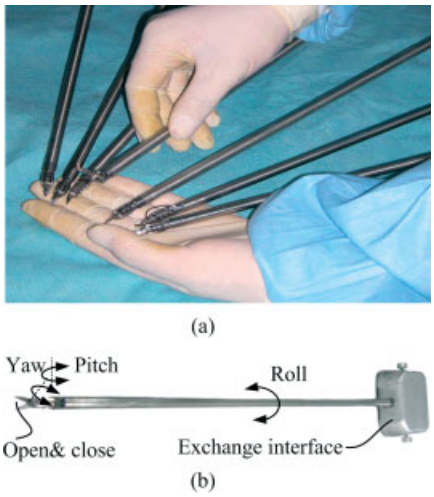

Figure 6. Multi-DOF instruments with a compact wrist mechanism: (a) multi-DOF instruments; (b) four-DOF scissors

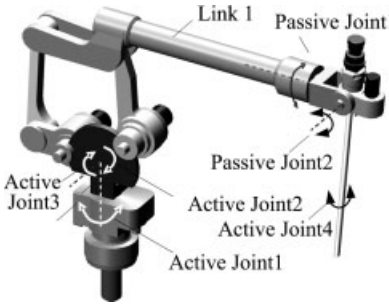

Figure 7. The slave endoscope manipulator

slave instrument manipulator. The prototype of the slave endoscope manipulator is shown in Figure 7. The holding endoscope part is composed of four active joints and two passive joints, applying the incision point as a fulcrum to realize the remote centre of motion. The first three DC servo-motors can be installed far from the patient for position adjustment and safety enhancement. The last DC servo-motor is installed at the end of the manipulator to realize the rotational motion of the endoscope around its axis. There are two passive joints set perpendicularly at the end of link I. The slave endoscope manipulator can be mounted on the passive base that could be adjusted before surgery.

Kinematics of the MicroHand A system

Using a tendon-driven system in the surgical robotic system has the advantages that the instruments can occupy a smaller space and have a lighter weight, and that the backlash is also minimized (19–23); thereby, robot-assisted minimally invasive surgery becomes possible. The kinematic behaviour of the master and the slave manipulators were analysed in order to implement motion control of the MicroHand A system.

The master forward kinematics

The teleoperation master is a serial robot. Gravity balance is achieved by the mechanical structure and translational motion in two directions, relative to the end of the reference point, is accomplished by the principle of the parallelogram. The naming convention and zero configuration are shown in Figure 8.

To construct the twists for the revolute joints, note that:

$$\boldsymbol{\omega}_1 = \boldsymbol{\omega}_2 = \boldsymbol{\omega}_4 = \boldsymbol{\omega}_6 = [0 \quad 0 \quad 1]^{\mathrm{T}},\ \boldsymbol{\omega}_3 = \boldsymbol{\omega}_5 = [1 \quad 0 \quad 0]^{\mathrm{T}} \tag{1}$$

and the axis points can be chosen as:

$$\boldsymbol{q}_1 = [0 \quad 0 \quad 0]^{\mathrm{T}},\ \boldsymbol{q}_2 = \boldsymbol{q}_3 = [l_1 \quad 0 \quad 0]^{\mathrm{T}},\ \boldsymbol{q}_4 = \boldsymbol{q}_5 = \boldsymbol{q}_6 = [l_1 - l_3 \quad -l_2 \quad 0]^{\mathrm{T}} \tag{2}$$

This yields the twists:

$$\hat{\boldsymbol{\xi}}_i = \begin{bmatrix} -\boldsymbol{\omega}_i \times \boldsymbol{q}_i \\ \boldsymbol{\omega}_i \end{bmatrix},\ i = 1, 2, \ldots, 6 \tag{3}$$

and the zero configuration:

$$\boldsymbol{g}_{mst}(\boldsymbol{0}) = \begin{bmatrix} & \boldsymbol{I}_{3\times 3} & & \begin{matrix} l_1 - l_3 \\ -l_2 \\ 0 \end{matrix} \\ 0 & 0 & 0 & 1 \end{bmatrix} \tag{4}$$

The forward kinematics map of the master manipulator has the form:

$$\boldsymbol{g}_{mst}(\boldsymbol{\theta}) = \begin{bmatrix} \boldsymbol{R}_m(\boldsymbol{\theta}) & \boldsymbol{p}_m(\boldsymbol{\theta}) \\ 0 & 1 \end{bmatrix} \tag{5}$$

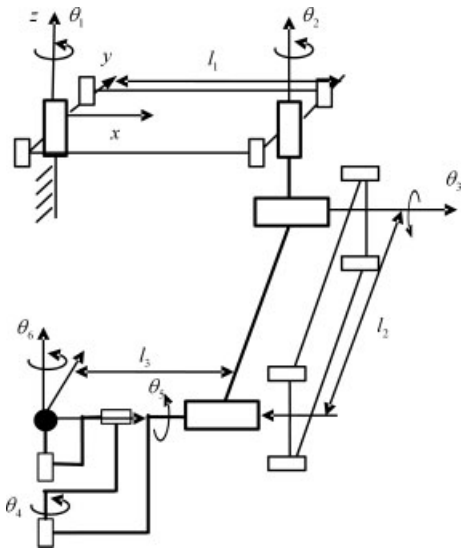

Figure 8. The naming convention and the zero configuration of the master manipulator

where $\boldsymbol{R}_m(\boldsymbol{\theta}) = e^{\hat{\omega}_2\theta_2} e^{\hat{\omega}_4\theta_4} e^{\hat{\omega}_5\theta_5} e^{\hat{\omega}_6\theta_6} \boldsymbol{I}_{3\times 3}$, $\boldsymbol{p}_m(\boldsymbol{\theta}) = H \left[e^{\hat{\xi}_1\theta_1} e^{\hat{\xi}_2(\theta_2-\theta_1)} \boldsymbol{g}_{mst}(0) \begin{bmatrix} 0 \\ 0 \\ 0 \\ 1 \end{bmatrix} \right]$, l_i and θ_i are the link length and the joint angle of the master manipulator, respectively.

The slave instrument manipulator forward kinematics

The passive part of the slave instrument manipulator is not controlled during surgery, thus only the kinematics of an active part with the remote centre of motion mechanism and a multi-DOF instrument was analysed. The active part consists of two translation joints and four revolution joints. The origin of the S frame is remote centre, which is a fixed point. In order to analyse this, translation joint d is converted into revolution joint θ_2. The naming convention and zero configuration are shown in Figure 9.

To construct the twists for the revolute joints, note that:

$$\boldsymbol{\omega}_1 = \boldsymbol{\omega}_6 = [1 \quad 0 \quad 0]^{\mathrm{T}},\quad \boldsymbol{\omega}_2 = \boldsymbol{\omega}_5 = [0 \quad 1 \quad 0]^{\mathrm{T}},\quad \boldsymbol{\omega}_4 = [0 \quad 0 \quad 1]^{\mathrm{T}},\quad \boldsymbol{v}_3 = [0 \quad 0 \quad 1]^{\mathrm{T}} \tag{6}$$

and the axis points are chosen as:

$$\boldsymbol{q}_1 = [0 \quad 0 \quad 0]^{\mathrm{T}},\quad \boldsymbol{q}_2 = \boldsymbol{q}_3 = \boldsymbol{q}_4 = [b \quad 0 \quad 0]^{\mathrm{T}},\quad \boldsymbol{q}_5 = [b \quad 0 \quad l_4]^{\mathrm{T}},\quad \boldsymbol{q}_6 = [b \quad 0 \quad l_4 + l_5]^{\mathrm{T}} \tag{7}$$

This yields twists:

$$\hat{\boldsymbol{\xi}}_i = \begin{bmatrix} -\boldsymbol{\omega}_i \times \boldsymbol{q}_i \\ \boldsymbol{\omega}_i \end{bmatrix},\quad i = 1, 2, 4, 5, 6 \quad \hat{\boldsymbol{\xi}}_3 = [0 \quad 0 \quad 1 \quad 0 \quad 0 \quad 0]^{\mathrm{T}} \tag{8}$$

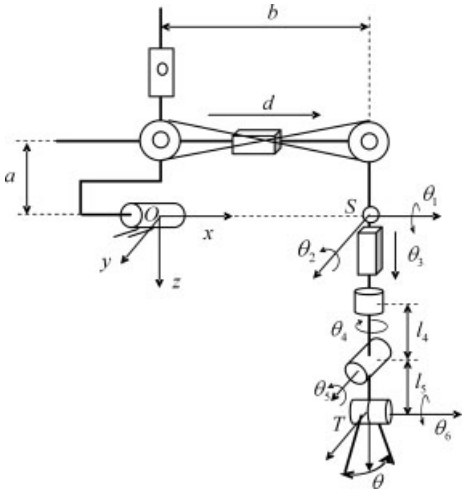

Figure 9. The naming convention and the zero configuration of the slave instrument manipulator

and the zero configuration:

$$g_{sst}(\boldsymbol{0}) = \begin{bmatrix} & \boldsymbol{I}_{3\times3} & & b \\ & & & 0 \\ & & & l_4 + l_5 \\ 0 & 0 & 0 & 1 \end{bmatrix} \tag{9}$$

The forward kinematics map of the manipulator has the form:

$$g_{sst}(\boldsymbol{\theta}) = \prod_{i=1}^{6} e^{\hat{\xi}_i \theta_i} g_{sst}(0) = \begin{bmatrix} \boldsymbol{R}_s(\boldsymbol{\theta}) & \boldsymbol{p}_s(\boldsymbol{\theta}) \\ 0 & 1 \end{bmatrix} \tag{10}$$

The slave instrument manipulator inverse kinematics

To decouple the tendon-driven joints and to accomplish control, the inverse kinematics of the slave instrument manipulator is analysed by the following two steps. The first step is to derive the relationship between the end effector and the joint angles of the slave instrument manipulator after removal of tendons and pulleys. The second step is to derive the relationship between the motor angle and the joint angle, using the tendon displacement and the corresponding joint angle.

The inverse kinematics problem is considered after removing tendons and pulleys: given a desired configuration for the tool frame, joint angles achieving that configuration are found. This means that, given a forward kinematics map $g_{st}(\boldsymbol{\theta}) : Q \to SE(3)\ \boldsymbol{\theta} \in Q$ and desired configuration $g_d \in SE(3)$, the equation is solved as:

$$\begin{aligned} g_{st}(\boldsymbol{\theta}) &= e^{\hat{\xi}_1\theta_1} e^{\hat{\xi}_2\theta_2} e^{\hat{\xi}_3\theta_3} e^{\hat{\xi}_4\theta_4} \\ & e^{\hat{\xi}_5\theta_5} e^{\hat{\xi}_6\theta_6} g_{st}(0) = g_d = \begin{bmatrix} \boldsymbol{w} & \boldsymbol{v} & \boldsymbol{u} & \boldsymbol{r} \\ 0 & 0 & 0 & 1 \end{bmatrix} \end{aligned} \tag{11}$$

The structure of the slave instrument manipulator with two prismatic joints and four revolute joints can not be fully solved through subproblems, according to Murray *et al*. (24). In this study, the last three joint angles can be solved through subproblems. Vector loop closure equations are partly used for the first three joints. The values for θ_1 and θ_2 can be obtained by the configuration shown in Figure 10.

$$\boldsymbol{r}_5 = \boldsymbol{r} - \boldsymbol{r}_s \tag{12}$$

$$\boldsymbol{r}_4 = \boldsymbol{r}_5 - l_5 \frac{\boldsymbol{w} \times \dfrac{\boldsymbol{r}_5 \times \boldsymbol{w}}{\|\boldsymbol{r}_5 \times \boldsymbol{w}\|}}{\left\| \boldsymbol{w} \times \dfrac{\boldsymbol{r}_5 \times \boldsymbol{w}}{\|\boldsymbol{r}_5 \times \boldsymbol{w}\|} \right\|} \tag{13}$$

$$\boldsymbol{w}_1 = \frac{\boldsymbol{r}_4}{\|\boldsymbol{r}_4\|} = e^{\hat{\omega}_1\theta_1} e^{\hat{\omega}_2\theta_2} \begin{bmatrix} 0 \\ 0 \\ 1 \end{bmatrix} \tag{14}$$

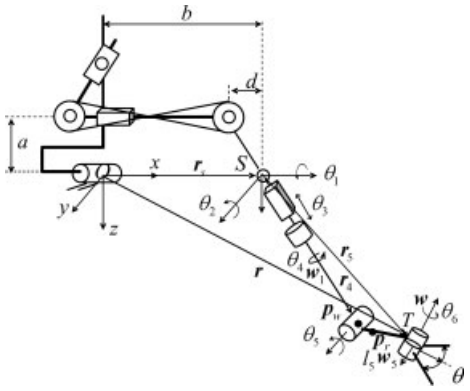

Figure 10. The general configuration of the slave instrument manipulator

According to structural characteristics, two prismatic joints are coupled, thus:

$$d = -a \tan\theta_2 \tag{15}$$

$$l = \theta_3 - \frac{a}{\cos\theta_2} \tag{16}$$

Since θ_1, θ_2 and θ_3 are known, the equation becomes:

$$e^{\hat{\xi}_4\theta_4} e^{\hat{\xi}_5\theta_5} e^{\hat{\xi}_6\theta_6} = e^{-\hat{\xi}_3\theta_3} e^{-\hat{\xi}_2\theta_2} e^{-\hat{\xi}_1\theta_1} g_d g_{st}^{-1}(0) =: g_1 \tag{17}$$

where θ_4, θ_5, θ_6 can be determined through the following two steps:

Step 1. Solve joint angle θ_6. Apply both sides of equation (17) to a point $\boldsymbol{p}_r \in R^3$ which is not on the axes of $\hat{\xi}_4, \hat{\xi}_5, \hat{\xi}_6$. This yields:

$$e^{\hat{\xi}_4\theta_4} e^{\hat{\xi}_5\theta_5} e^{\hat{\xi}_6\theta_6} \boldsymbol{p}_r = g_1 \boldsymbol{p}_r \tag{18}$$

Subtracting the intersection of the axes of $\hat{\xi}_4$ and $\hat{\xi}_5$ from both sides of equation (18) and taking the magnitude of both sides of the equation yields:

$$\begin{aligned} & e^{\hat{\xi}_4\theta_4} e^{\hat{\xi}_5\theta_5} e^{\hat{\xi}_6\theta_6} \boldsymbol{p}_r - \boldsymbol{p}_w \\ & \quad = e^{\hat{\xi}_4\theta_4} e^{\hat{\xi}_5\theta_5} (e^{\hat{\xi}_6\theta_6} \boldsymbol{p}_r - \boldsymbol{p}_w) = g_1 \boldsymbol{p}_r - \boldsymbol{p}_w \end{aligned} \tag{19}$$

and:

$$\left\| e^{\hat{\xi}_6\theta_6} \boldsymbol{p}_r - \boldsymbol{p}_w \right\| = \|g_1 \boldsymbol{p}_r - \boldsymbol{p}_w\| \tag{20}$$

where $\boldsymbol{p}_w$ is the intersection of the axes of $\hat{\xi}_4$ and $\hat{\xi}_5$. Using the property that the distance between points is preserved by rigid motion, θ_6 can be solved by applying subproblem 3.

Step 2. Solve angle θ_4 and angle θ_5. Since θ_6 is known, equation (18) becomes:

$$e^{\hat{\xi}_4\theta_4} e^{\hat{\xi}_5\theta_5} (e^{\hat{\xi}_6\theta_6} \boldsymbol{p}_r) = g_1 \boldsymbol{p}_r \tag{21}$$

The values for θ_4 and θ_5 can be obtained by applying subproblem 2.

In order to facilitate analysis, the tendon-driven multi-DOF instrument obeys the following assumptions (25–27):

1. All tendons are under tension and the stretch is ignored.
2. There is no slippage between pulley and tendon.

The transmission schematic of the tendon-driven instrument is shown in Figure 11. The relationship between the displacement of the tendons and the joint angles can be described by the following equation according to the transmission principle of tendons:

$$\boldsymbol{s} = \boldsymbol{A}\boldsymbol{\theta} \tag{22}$$

where $\boldsymbol{s} = [s_1 \quad s_2 \quad s_3 \quad s_4 \quad s_5 \quad s_6 \quad s_7 \quad s_8]^{\mathrm{T}}$ is an 8×1 tendon displacement vector, $\boldsymbol{\theta} = [\theta_5 \quad \theta_6 \quad \theta_4]^{\mathrm{T}}$ is a 3×1 joint angle vector, and $\boldsymbol{A} = \begin{bmatrix} r_1 & 0 & 0 \\ -r_1 & 0 & 0 \\ r_5 & r_3 & 0 \\ -r_7 & -r_3 & 0 \\ r_4 & r_2 & 0 \\ -r_6 & -r_2 & 0 \\ 0 & 0 & r_8 \\ 0 & 0 & -r_8 \end{bmatrix}$ is an 8×3 matrix about the radius of the pulleys pivoted about the corresponding joint axis.

It can be seen from Figure 11 that the rotor angular displacement of the motor, θ_{mi}, can be related to the tendon displacement, s_i, by:

$$\frac{\theta_{mi}}{n_i} r_{mi} = s_i \tag{23}$$

where n_i is a gear reduction ratio of the ith speed reducer and r_{mi} is the radius of the pulley pivoted about the output axis of the ith speed reducer.

Thus, the relationship between the rotor angular displacements of the motors and the joint angles can be depicted by:

$$\boldsymbol{A}\boldsymbol{\theta} = \boldsymbol{R}_{\boldsymbol{mi}}\boldsymbol{\theta}_{\boldsymbol{mi}} \tag{24}$$

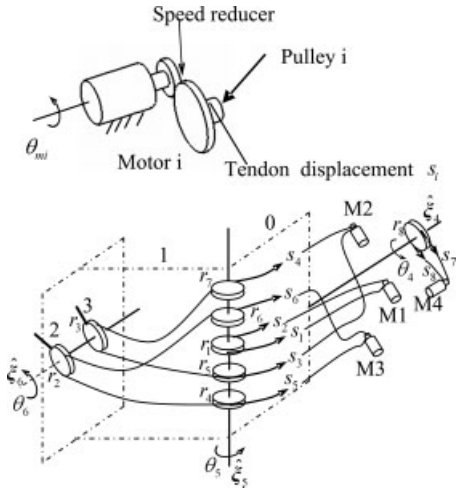

Figure 11. The transmission schematic of the tendon-driven instrument

where $\boldsymbol{R}_{mi} = diag\left\{\frac{r_{m1}}{n_1} \quad \frac{r_{m1}}{n_1} \quad \frac{r_{m2}}{n_2} \quad \frac{r_{m2}}{n_2} \quad \frac{r_{m3}}{n_3} \quad \frac{r_{m3}}{n_3} \quad \frac{r_{m4}}{n_4} \quad \frac{r_{m4}}{n_4}\right\}$ is an 8×8 matrix, n_i, $i = 1,2,3,4$ is the gear reduction ratio, r_{mi}, $i = 1,2,3,4$ is the radius of the pulley pivoted about the output axis of the corresponding speed reducer, and $\boldsymbol{\theta}_{\boldsymbol{mi}} = [\theta_{m1} \quad -\theta_{m1} \quad \theta_{m2} \quad -\theta_{m2} \quad \theta_{m3} \quad -\theta_{m3} \quad \theta_{m4} \quad -\theta_{m4}]^{\mathrm{T}}$ is an 8×1 motor angular displacement vector.

Intuitive control algorithm

When operating the master and slave manipulators, the surgeon must operate the master manipulator within limit of the reachable workspace. Hence, when the master manipulator goes beyond its workspace, the surgeon must disconnect master–slave operation to reposition the master manipulator and make the workspace of the master manipulator match well with that of the slave to improve manoeuvrability. It is especially useful when motion scaling is carried out. Motion scaling can allow large master manipulator motion to correspond to small slave manipulator motion, making the slave manipulator steady even under jerky master manipulator movements. Alignment of the visual image of tip motion of the slave instrument manipulator on the monitor and that of the hand motion of the surgeon must be implemented in order to accomplish intuitive control. Intuitive control under 1 : 1 master–slave scaling mode can be written as follows:

$$\boldsymbol{g}_{\boldsymbol{ET}}(t) = \boldsymbol{g}_{\boldsymbol{DH}}(t) \tag{25}$$

where $\boldsymbol{g}_{\boldsymbol{ET}}(t) = \boldsymbol{g}_{\boldsymbol{ES}}\boldsymbol{g}_{\boldsymbol{ST}}(t)$ and $\boldsymbol{g}_{\boldsymbol{DH}}(t) = \boldsymbol{g}_{\boldsymbol{DM}}\boldsymbol{g}_{\boldsymbol{MH}}(t)$ are motion trajectories of the instrument end-effector at endoscope frame E and the master manipulator end-effector at monitor frame D, respectively. $\boldsymbol{g}_{\boldsymbol{ES}}$ and $\boldsymbol{g}_{\boldsymbol{DM}}$ are coordinate transformations from the slave manipulator frame S to the endoscope frame E and from the master manipulator frame M to the monitor frame D, respectively.

In order to better describe intuitive control and motion scaling control in master–slave mode, the mapping relation can be expressed as:

$$\begin{bmatrix} {}^{S}_{T}\boldsymbol{R}_{\boldsymbol{i}} & {}^{S}_{T}\boldsymbol{P}_{\boldsymbol{i}} \\ 0 & 1 \end{bmatrix} = \begin{bmatrix} {}^{E}_{S}\boldsymbol{R}_{\boldsymbol{i}}^{-1}\,{}^{D}_{M}\boldsymbol{R}_{\boldsymbol{i}}\,{}^{M}_{H}\boldsymbol{R}_{\boldsymbol{i}} & {}^{S}_{T}\boldsymbol{P}_{\boldsymbol{i-1}} + K_p l\,{}^{E}_{S}\boldsymbol{R}_{\boldsymbol{i}}^{-1}\,{}^{D}_{M}\boldsymbol{R}_{\boldsymbol{i}}\,{}^{M}_{H}\boldsymbol{\Delta P}_{\boldsymbol{i}} \\ 0 & 1 \end{bmatrix} \tag{26}$$

where ${}^{S}_{T}\boldsymbol{P}_{\boldsymbol{i}}$, ${}^{S}_{T}\boldsymbol{P}_{\boldsymbol{i-1}}$ and ${}^{S}_{T}\boldsymbol{R}_{\boldsymbol{i}}$ are the position and posture of the slave manipulator tool frame T relative to the slave manipulator frame S at the ith time step and the $(i-1)$th time step, respectively; ${}^{M}_{H}\boldsymbol{\Delta P}_{\boldsymbol{i}} = ({}^{M}_{H}\boldsymbol{P}_{\boldsymbol{i}} - {}^{M}_{H}\boldsymbol{P}_{\boldsymbol{i-1}})$ and ${}^{M}_{H}\boldsymbol{R}_{\boldsymbol{i}}$ are the position increment and posture of the master manipulator end-effector frame H relative to master manipulator frame M at the ith time and the $(i-1)$th time, respectively; ${}^{E}_{S}\boldsymbol{R}$ describes the rotation of the slave manipulator frame S relative to the endoscope frame E; ${}^{D}_{M}\boldsymbol{R}$ describes the rotation of the master manipulator

DOI: 10.1002/rcs

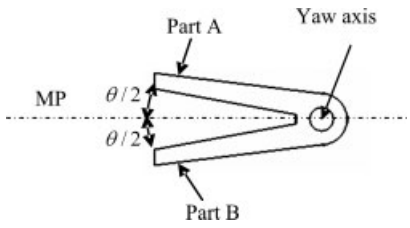

Figure 12. Open-and-close implementation

frame M relative to the monitor frame D; K_p is the motion scaling factor selected by the task requirement; and l is the master–slave connection factor, $l = \begin{cases} 0 & \text{disconnection} \\ 1 & \text{connection} \end{cases}$.

Open-and-close algorithm

Figure 12 shows the open-and-close implementation of instruments. The end-effector consists of parts A and B. Both of them move toward or away from the middle plane (MP), where the open-and-close operation is performed. While they move in the same direction, the joint angle is defined as the rotation angle of the middle plane around the yaw axis.

Thus, the relationship of the rotor angular displacements of the motors, the joint angles and the open-and-close angle can be written as:

$$\begin{bmatrix} r_1 & 0 & 0 & 0 \\ -r_1 & 0 & 0 & 0 \\ r_5 & r_3 & 0 & r_3/2 \\ -r_7 & -r_3 & 0 & -r_3/2 \\ r_4 & r_2 & 0 & -r_2/2 \\ -r_6 & -r_2 & 0 & r_2/2 \\ 0 & 0 & r_8 & 0 \\ 0 & 0 & -r_8 & 0 \end{bmatrix} \begin{bmatrix} \theta_5 \\ \theta_6 \\ \theta_4 \\ \theta \end{bmatrix} = \boldsymbol{R}_{mi}\boldsymbol{\theta}_{mi} \qquad (27)$$

Control system design

The overall architecture of the control system for the MicroHand A system has been developed, as shown in Figure 13.

The control system uses a modular design. It consists of a human–machine interface, three sets of single-board PMACs and several motor controllers. The single-board PMAC is used as a high-level controller and each motor controller is used as low-level controller. Each set includes a single-board PMAC and seven or ten motor controllers.

Human–machine interface

The human–machine interface is used for parameter setting, mode selection, surgeon training and data display, including work status information and warning or error information. A redundant user command interface has also been designed in the MicroHand A system. In the controller, redundant user commands have response priority over other control commands to ensure the reliability and safety of the whole system.

High-level controller

The high-level controller achieves the master–slave teleoperation control, which includes position and posture information acquisition of the master manipulator, motion control of the slave manipulator, kinematics calculations of the master and slave manipulator, master–slave control algorithm implementation, and I/O control. The controller is programmed to respond to commands from master manipulator motion or digital inputs, such as a button and a pedal. It is also programmed to send appropriate control signals and commands to the

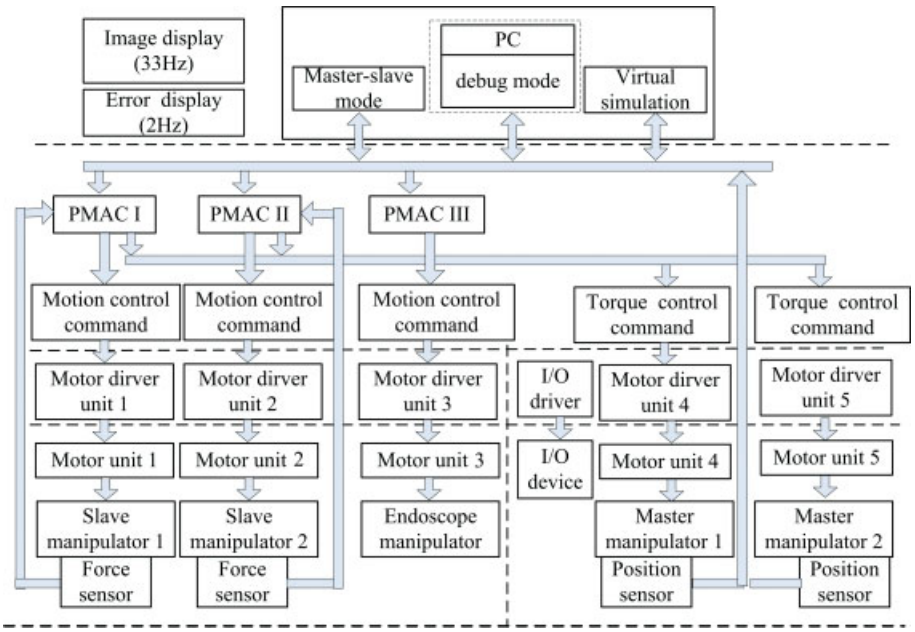

Figure 13. The overall architecture of control system for the MicroHand A system

DOI: 10.1002/rcs

motor controllers or output digital information, such as status and warning information. At present, the master manipulator is mainly used to acquire the surgeon's hand position and posture information. The force feedback function is reserved, because force information is missed in the slave instrument manipulator. The motion of the slave instrument or endoscope manipulators can be controlled by the servo-motors installed at the joints of the manipulator. The slave manipulators can be moved according to the motion of the master manipulator.

Low-level controller

Each motor controller used as low-level controller executes proportional–integral feedback gain control. The motor controllers can be operated in position, velocity and torque modes. The control commands can be given by analogue voltage, pulse-width modulation, serial port or Ethernet port commands.

Master–slave control for the MicroHand A system

Current implementation of master–slave control for the MicroHand A system is shown in Figure 14, where the force feedback function is reserved. Joint angle control is used in the control system. Determined by an intuitive master–slave control algorithm, each joint of the slave manipulator is controlled by a PD controller to follow the trajectory of the teleoperation master manipulator directly produced by the surgeon.

Stability analysis

A bilateral teleoperation system can be presented with a two-port network relating velocity/position and force at the master and slave sides (28,29). According to the impedance parameters of the two-port network theory, the master–slave teleoperation system can be expressed as:

$$\begin{bmatrix} F_h(s) \\ -F_e(s) \end{bmatrix} = \begin{bmatrix} z_{11}(s) & z_{12}(s) \\ z_{21}(s) & z_{22}(s) \end{bmatrix} \begin{bmatrix} \dot{X}_m(s) \\ \dot{X}_s(s) \end{bmatrix} \tag{28}$$

Stability and transparency are two major issues in teleoperation systems. The stability of the master–slave system can be analysed under the condition that the operator and the environment are passive. The necessary and sufficient conditions for absolute stability in terms of the z parameters are:

1. $z_{11}(s)$ and $z_{22}(s)$ have no poles in the right half-plane.
2. Any pole of $z_{11}(s)$ and $z_{22}(s)$ on the imaginary axis is simple with real and positive residues.
3. For all real values:

$$\begin{aligned} &\mathrm{Re}[z_{11}(s)] \geq 0 \\ &\mathrm{Re}[z_{22}(s)] \geq 0 \\ &2\mathrm{Re}[z_{11}(s)]\mathrm{Re}[z_{22}(s)] - \mathrm{Re}[z_{12}(s)z_{21}(s)] \\ &\quad - |z_{12}(s)z_{21}(s)| \geq 0 \end{aligned} \tag{29}$$

The three conditions constitute Llewellyn's absolute stability criterion. If any of the conditions are not met, the network is potentially unstable.

When the master–slave manipulator's dynamic models are decoupled, the system is simplified to one DOF. this brings much convenience into analysis. Dynamic models of one DOF master–slave manipulators are used in this section as the basis of analysis. Assuming that measuring interaction by force sensors between the slave manipulator and environment is fed back to the master manipulator, the dynamic model of the master manipulator can be expressed as:

$$M_m\ddot{x}_m(t) + B_m\dot{x}_m(t) = F_h(t) - K_f F_e(t - T_2) \tag{30}$$

The dynamic model of the slave manipulator can be written as:

$$M_s\ddot{x}_s(t) + B_s\dot{x}_s(t) = F_s(t) - F_e(t) \tag{31}$$

The control force model of the slave manipulator is:

$$F_s(t) = K_c(K_p x_m(t - T_1) - x_s(t)) \tag{32}$$

where M_m, M_s, $x_m(t)$, $x_s(t)$, B_m, and B_s are qualities, positions and dampings of the master manipulator and the slave manipulator, respectively; $F_h(t)$ is the contact force between the master manipulator and human operator;

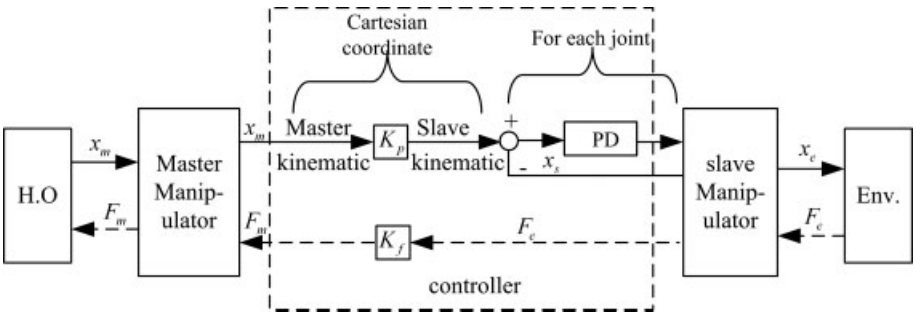

Figure 14. The master–slave control for the MicroHand A system

$F_e(t)$ is the contact force between the environment and the slave manipulator; $F_s(t)$ is the control force of the slave manipulator; T_1 and T_2 are time delays from the master side to the slave side and reverse; K_c is the proportion parameter of the controller at the slave; and K_f and K_p are scaling factors for force and position, respectively.

Taking the Laplace transform of equations (30), (31) and (32) and combining them with equation (28), the impedance matrix can be obtained as:

$$Z = \begin{bmatrix} z_{11}(s) & z_{12}(s) \\ z_{21}(s) & z_{22}(s) \end{bmatrix} = \begin{bmatrix} M_m s + B_m + \dfrac{K_c K_f K_p e^{-(T_1+T_2)s}}{s} \\ K_f(M_s s + B_s + \dfrac{K_c}{s})e^{-T_2 s} \\ \dfrac{K_c K_p e^{-T_1 s}}{s} \\ M_s s + B_s + \dfrac{K_c}{s} \end{bmatrix} \quad (33)$$

Obviously, the poles of $z_{11}(s)$ and $z_{22}(s)$ are zero and the poles of $z_{11}(s)$ and $z_{22}(s)$ on the imaginary axis are simple, with real and positive residues $K_c K_f K_p$ and K_c. Hence, the first two conditions of Llewellyn's absolute stability criterion are met. In order to satisfy the third condition of Llewellyn's absolute stability criterion, the following conditions should be met:

$$\begin{aligned} &B_m > \frac{K_c K_f K_p \sin((T_1+T_2)\omega)}{\omega} \\ &B_s > 0 \\ &B_m B_s \geq \frac{K_c K_f K_p}{\omega}\left[\frac{3}{2}B_s \sin(\omega(T_1+T_2)) + \frac{1}{2}(M_s\omega - \frac{K_c}{\omega})\right. \\ &\left.\cos(\omega(T_1+T_2)) + \frac{1}{2}\sqrt{B_s^2 + (M_s\omega - \frac{K_c}{\omega})^2}\right] \end{aligned} \quad (34)$$

In a word, suitable parameters can be found to satisfy Llewellyn's absolute stability criterion. The stability of the system can be therefore guaranteed.

Transparency analysis

In this section, qualitative transparency analysis is carried out due to the absence of a force sensor in the slave manipulator. Assuming that $Z_m = M_m s + B_m$, $Z_s = M_s s + B_s$ and $Z_f = \frac{K_c}{s}$ are damps at the master side, the slave side and the controller for the slave side, respectively, and that $Z_e = \frac{F_e}{V_s}$ and $Z_h = \frac{F_h}{V_m}$ are the impedances of the environment and the human operator, the following equation can be obtained according to equation (33):

$$Z_h = Z_m + \frac{K_f K_p Z_e Z_f e^{-s(T_1+T_2)}}{Z_e + Z_s + Z_f} \quad (35)$$

The transparency of two extreme situations will be analysed:

1. Slave manipulator in free space motion, $Z_e \to 0$. Substituting $Z_e \to 0$ into equation (35), it can be rewritten as:
$$Z_h = Z_m \quad (36)$$
As the human operator's impedance is equal to the master manipulator impedance, the system can not be transparent completely.
2. Hard contact between the slave manipulator and the environment, $Z_e \to \infty$. Substitute $Z_e \to \infty$ into equation (35), it can be rewritten as:
$$Z_h = Z_m + \frac{K_f K_p Z_f e^{-s(T_1+T_2)}}{1 + \dfrac{Z_s}{Z_e} + \dfrac{Z_f}{Z_e}} \approx Z_m + K_f K_p Z_f e^{-s(T_1+T_2)} \quad (37)$$
To have better transparency, $K_f K_p Z_f$ should be as large as possible for constant Z_m.

Experiments and Results

Some experiments have been designed and carried out to verify the performance of the control system of the MicroHand A system.

Tracking response experiment

The slave manipulator is moved by controlling motors installed at the corresponding joints according to the target position information from the master manipulator. The joint input of the slave manipulator is the given joint position, which is calculated by using the slave manipulator inverse kinematics according to the master manipulator's forward kinematics given position.

The task of picking up a washer from a screw bolt and putting the washer on the screw bolt was realized. Figure 15 shows the tracking response experiment, where the desired trajectory was commanded by the master manipulator and the actual trajectory of the slave manipulator was in the joint space. The root mean square error of trajectory tracking for each joint is given in Table 1. It can be seen from Figure 15 and Table 1 that the MicroHand A system achieves excellent tracking performance.

Gall bladder removal experiment

A series of experiments of gall bladder removal on pig were successfully implemented at Tianjin University. The whole process is shown in Figure 16. The experiment includes separation of the cystic duct, ligation of the cystic duct, separation of the gall bladder, and removal of the gall bladder. During separation of the cystic duct, the common bile duct, the right hepatic duct and the right hepatic artery were not injured. The experiment shows that the MicroHand A system has high operating and control precision. The control system can eliminate manual tremor and achieve much finer and smoother trajectory by introducing scaling motion control. It took approximately 3 min to knot the cystic duct. The MicroHand A system

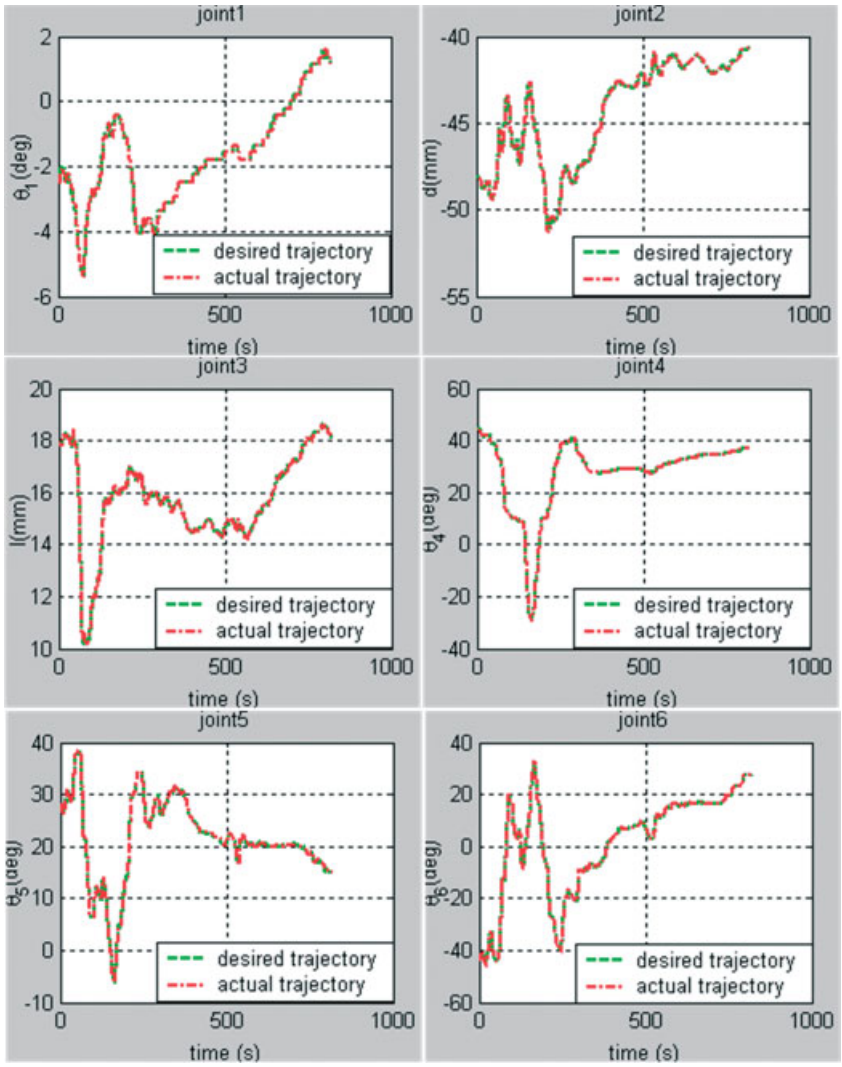

Figure 15. Tracking response between the desired trajectory commanded by the master and the actual trajectory of the slave

was proved to have sufficient dexterity and the force of the instrument tip is large enough for knot-tying. Intuitive motion control and scaling motion control were adopted to solve problems caused by the master–slave mode, including absonant hand–eye coordination, kinematical dissimilarity and workspace mismatch. Gall bladder removal experiments were successfully performed on a pig. After surgery, the pigs were in good condition without any disease complications, demonstrating the feasibility of the MicroHand A system for clinical applications. The failure rates of hardware and software for the MicroHand A system were zero during all experiments, indicating that the control system, including software and hardware, is stable and reliable.

Table 1. The root mean square error of trajectory tracking for each joint

RMS	θ_1 (°)	d (mm)	l (mm)	θ_4 (°)	θ_5 (°)	θ_6 (°)
	0.0850	0.1350	0.0601	0.1986	0.2250	0.2968

Discussion

Compared with traditional minimally invasive surgery, robot-assisted minimally invasive surgery provides the surgeon with better control over surgical instruments and a better 3D view of the surgical site. In addition, surgeons no longer have to stand beside the operating table throughout the whole surgery and hand tremors can also be filtered out by the control system. According to design requirements in robot-assisted laparoscopic surgery, a robot-assisted minimally invasive surgery system named MicroHand A has been designed and implemented at Tianjin University. It consists of two master manipulators, two slave instrument manipulators and one endoscope manipulator. Kinematic analysis of the MicroHand A system has been derived for control purposes. The master–slave control system with intuitive motion control and motion scaling control have been designed and implemented. The stability and transparency of the system were analysed, assuming that dynamics of each joint is decoupled. Conditions satisfying Llewellyn's absolute stability criterion were derived and

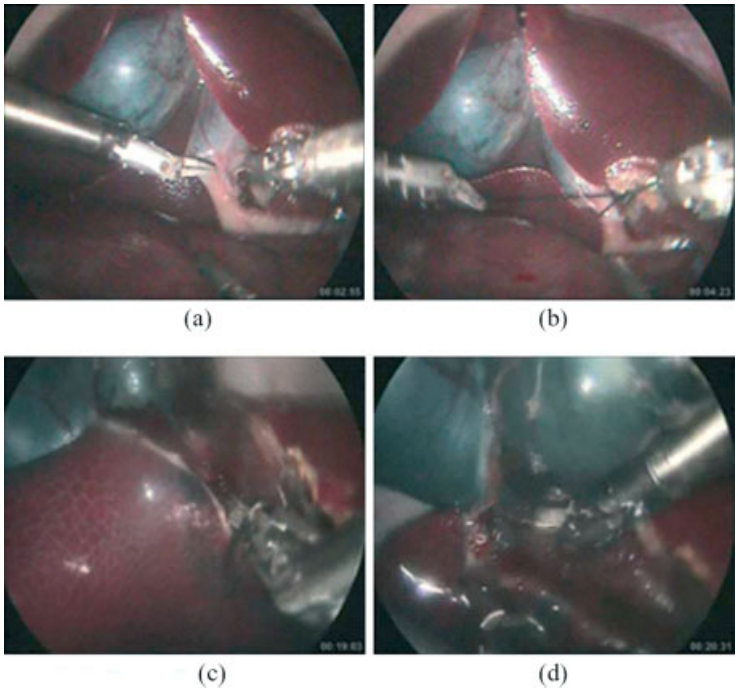

Figure 16. The gall bladder removal experiment on a pig: (a) separating the cystic duct; (b) knotting the cystic duct; (c) separating the gall bladder; (d) removing the gall bladder

the transparency of two extreme situations was analysed. A series of experiments were designed and carried out to verify the performance of the MicroHand A control system.

The forward and inverse kinematics of the MicroHand A system were derived by the screw theory and the part-vector loop equation. The tendon-driven mechanism adopted in the MicroHand A system causes coupling among joints. For control and decoupling purposes, the relationships among actuator space, the Cartesian space and joint space were derived.

In order to implement intuitive control and scaling control, an intuitive control algorithm has been designed and implemented to solve absonant hand–eye coordination, kinematical dissimilarity and workspace mismatch. Meanwhile, an open-and-close algorithm has been proposed to grasp tissues, sutures and needles.

The control system for the MicroHand A system consists of a human–machine interface, a high-level controller and a low-level controller. It has been modularly developed and implemented for easy use, maintenance and upgrading.

To analyse the stability and transparency of the control system, a two-port network theory was used to describe the MicroHand A system. Dynamic models of the one-DOF master manipulator and the one-DOF slave manipulator were used to analyse stability and transparency under the assumption that the dynamic model of each joint is decoupled. According to the impedance parameters of the two-port network theory, conditions that satisfy Llewellyn's absolute stability criterion are derived and the transparency of two extreme situations were qualitatively analysed, since the force sensor is absent in the slave manipulator. It was found that the system can not be transparent completely when the slave manipulator moves freely, and that parameters $K_f K_p Z_f$ should be as large as possible when there is a hard contact between the slave manipulator and environment. The force feedback to the human operator is large.

A series of experiments, including tracking response and a gall bladder removal experiment on a pig were successfully carried out under the master–slave control mode. The results show that the MicroHand A system eliminates manual tremor and achieves a fine and smooth trajectory by introducing scaling factors between the operator's hand motion and the motion of the instruments. It is also indicated that multi-DOF instruments provide sufficient dexterity for complex surgery, such as suturing and knot-tying. The control system of the MicroHand A system that involves intuitive motion control and scaling motion control was verified to be stable and reliable. The MicroHand A system has the potential for clinical application with further improvement.

Further testing, tuning and optimization of the MicroHand A system are needed to improve performance, such as the response time, error compensation and safety issues under clinical circumstances. Sensing and force feedback is also expected to be introduced into the MicroHand A system. Future experiments will be done on force tracking by obtaining force information from the slave manipulator and will be extended to the whole robotic system.

Acknowledgements

This study was supported by the National Science Foundation of China (NSFC; Grant No. 50925520) and the National High Technology Foundation '863' Project (Grant No. 2009AA044001).

Appendix

1. The closed form of the forward kinematics of the master manipulator is written as:

$$g_{mst}(\theta) = \begin{bmatrix} R_m(\theta) & p_m(\theta) \\ 0 & 1 \end{bmatrix} = \begin{bmatrix} (c_2c_4-s_2s_4)c_6 & -(c_2c_4-s_2s_4)s_6 & (s_2c_4+c_2s_4)s_5 & l_1c_1+l_2s_2c_3-l_3c_2 \\ -(s_2c_4+c_2s_4)c_5c_6 & (c_2s_4+s_2c_4)c_5c_6 & -(c_2c_4-s_2s_4)s_5 & l_1s_1-l_2c_2c_3-l_3s_2 \\ (s_2c_4+c_2s_4)c_6 & -(s_2c_4+c_2s_4)s_6 & c_5 & -l_2s_3 \\ +(c_2c_4-s_2s_4)c_5s_6 & +(c_2c_4-s_2s_4)c_5c_6 & & \\ s_5s_6 & s_5c_6 & c_5 & 1 \\ 0 & 0 & 0 & \end{bmatrix}$$

where $s_i = \sin\theta_i$, $c_i = \cos\theta_i$.

2. The closed form of the forward kinematics of the slave manipulator is written as:

$$g_{sst}(\theta) = \begin{bmatrix} R_s(\theta) & p_s(\theta) \\ 0 & 1 \end{bmatrix} = \begin{bmatrix} r_{s11} & r_{s12} & r_{s13} & p_{sx} \\ r_{s21} & r_{s22} & r_{s23} & p_{sy} \\ r_{s31} & r_{s32} & r_{s33} & p_{sz} \\ 0 & 0 & 0 & 1 \end{bmatrix}$$

where:

$$\begin{aligned}
r_{s11} &= c_2c_4c_5 - s_2s_5 \\
r_{s12} &= s_1s_2c_4c_5 + c_1s_4c_5 + s_1c_2s_5 \\
r_{s13} &= s_1s_4c_5 - c_1(s_2c_4c_5 + c_2s_5) \\
r_{s21} &= s_2c_5s_6 + c_2(c_4s_5s_6 - s_4c_6) \\
r_{s22} &= c_1(c_4c_6 + s_4s_5s_6) - s_1(s_2s_4c_6 + (c_2c_5 - s_2c_4s_5)s_6) \\
r_{s23} &= c_6(s_1c_4 + c_1s_2s_4) + (s_1s_4s_5 + c_1(c_2c_5 - s_2c_4s_5))s_6 \\
r_{s31} &= s_2c_5c_6 + c_2(c_4s_5c_6 + s_4s_6) \\
r_{s32} &= c_4(s_1s_2s_5c_6 - c_1s_6) - s_1c_2c_5c_6 + s_4(c_1s_5c_6 + s_1s_2s_6) \\
r_{s33} &= s_1(s_4s_5c_6 - c_4s_6) + c_1(c_2c_5c_6 - s_2(c_4s_5c_6 + s_4s_6)) \\
p_{sx} &= b + (l_4 + \theta_3 + l_5c_5)s_2 + l_5c_2c_4s_5 \\
p_{sy} &= l_5(s_1s_2c_4 + c_1s_4)s_5 - c_2(l_4 + \theta_3 + l_5c_5)s_1 \\
p_{sz} &= l_5s_1s_4s_5 + c_1(c_2(l_4 + \theta_3 + l_5c_5) - l_5s_2c_4s_5) \\
s_i &= \sin\theta_i,\ c_i = \cos\theta_i.
\end{aligned}$$

and l_i and θ_i are the link length and the joint angle of the slave instrument manipulator, respectively.

References

1. Sun LW, Van Meer F, Schmid J, *et al*. Advanced da Vinci surgical system simulator for surgeon training and operation planning. *Int J Med Robotics Comput Assist Surg* 2007; **3**: 245–251.
2. Guthart GS, Salisbury JK. The Intuitive™ telesurgery system: overview and application. In Proceedings of the IEEE International Conference on Robotics and Automation, San Francisco, CA, USA, April 2000; 618–621.
3. Ghodoussi M, Butner SE, Wang YL. Robotic surgery – the transatlantic case. In Proceedings of the IEEE International Conference on Robotics and Automation, Washington, DC, USA, May 2002; 1882–1888.
4. Loulmet D, Carpentier A, d'Attellis N, *et al*. Total endoscopic computer enhanced coronary artery bypass grafting. *Eur J Cardiothorac Surg* 2000; **17**(1): 38–45.
5. Loulmet D, Carpentier A, d'Attellis N, *et al*. First endoscopic coronary artery bypass grafting using computer assisted instruments. *J Thoracic Cardiovasc Surg* 1999; **118**(1): 4–10.
6. Intuitive Surgical: http://www. intuitivesurgcial. com.
7. Sung G, Gill I. Robotic laparoscopic surgery: a comparison of the da Vinci and Zeus systems. *Urology* 2001; **58**(6): 893–898.
8. Cavusoglu ME, Tendick F, Cohn M, *et al*. A laparoscopic telesurgical workstation. *IEEE Trans Robotics* 1999; **15**(4): 728–739.
9. Kwon DS, Song SK. A microsurgical telerobot system with a 6-DOF haptic master device. In Proceedings of the International Symposium on Mechatronics and Intelligent Mechanical System for the 21st Century, Kyongsang Nam-Do, Korea, 4–7 October 2000; 65–71.
10. Hennann R. ARTEWS: a telemanipulator for cardiac surgery. *Eur J Cardiothorac Surg* 1999; **16**: S106–111.
11. Schurr MO, Buess G, Neisius B, *et al*. Robotics and telemanipulation technologies for endoscopic surgery, a review of the ARTEMIS project. *Surg Endosc* 2000; **14**(4): 375–381.
12. Ikuta K, Hasegawa T, Daifu S. Hyperredundant miniature manipulator 'Hyper Finger' for remote minimally invasive surgery in a deep area. In Proceedings of the IEEE International Conference on Robotics and Automation; 14–19 September 2003; 1098–1102.
13. Ikuta K, Yamamoto K, Sasaki K. Development of remote microsurgery robot and new surgical procedure for deep and narrow space. In Proceedings of the IEEE International Conference on Robotics and Automation, 14–19 September 2003; 1103–1108.
14. Nawrat Z, Podsedkowski L, Mianowski K, *et al*. RobIn Heart in 2002 – actual state of the Polish Cardia robot. In Proceedings of the Third International Workshop on Robot Motion and Control, 9–11 November 2002; 33–38.
15. Locke RCO, Patel RV. Optimal remote center-of-motion location for robotics-assisted minimally invasive surgery. In Proceedings of the IEEE International Conference on Robotics and Automation, Rome, Italy, 10–14 April 2007; 1900–1905.
16. Madhani AJ, Niemeyer G, Salisbury JK. The black falcon: a teleoperated surgical instrument for minimally invasive surgery. In Proceedings of the IEEE/RSJ International Conference on Intelligent Robots and Systems, 1998; 936–944.
17. Hamlin GJ, Sanderson AC. A novel concentric multilink spherical joint with parallel robotics applications. In Proceedings of the IEEE International Conference on Robotics and Automation, 1994; 1267–1272.
18. Li JM, Wang SX, Wang XF, *et al*. Optimization of a novel mechanism for a minimally invasive surgery robot. *Int J Med Robotics Comput Assist Surg* 2010; **6**: 83–90.
19. Tsai LW. *Robotic Analysis: The Mechanics of Serial and Parallel Manipulators*. Wiley: New York, 1999.
20. Salisbury JK. Kinematic and Force Analysis of Articulated Hands. Dissertation, Stanford University, CT, USA, 1982.
21. Albus J, Bostelman R, Dagalakis N. The NIST Spider, A Robot Crane. *J Res NIST* 1992; **97**(3): 373–385.
22. Kawamura S, Choe W, Tanaka S, *et al*. Development of an ultra-high-speed robot, FALCON, using a wire drive system. IEEE International Conference on Robotics and Automation, 1995; 215–220.
23. Jacobsen SC, Wood JE, Knutti DF, *et al*. The Utah–MIT dexterous hand: work in progress. *Int J Robotics Res* 1985; **3**(4): 21–50.

24. Murray RM, Li ZX, Shankar Sastry S. *A Mathematical Introduction to Robotic Manipulation*. CRC Press: Boca Raton, 1993.
25. Li C, Rahn CD. Design of continuous-backbone, cable-driven robots. *ASME J Mech Design* 2002; **124**(2): 265–271.
26. Lee JJ, Lee YH. Dynamic analysis of tendon-driven robotic mechanisms. *J Robotic Syst* 2003; **20**(5): 229–238.
27. Chang SL, Lee JJ, Yen,HC. Kinematic and compliance analysis for tendon-driven robotic mechanisms with flexible tendons. *Mechanism Machine Theory* 2005; **40**(6): 728–739.
28. Hannaford B. A design framework for teleoperators with kinesthetic feedback. *IEEE Trans Robot Autom* 1989; **5**(4): 426–434.
29. Hashtrudi-Zaad K, Salcudean SE. Analysis of control architectures for teleoperation systems with impedance/admittance master and slave manipulators. *Int J Robotics Res* 2001; **20**(6): 419–445.